



# A study on the complex dielectric ( $\epsilon^*$ )/electric-modulus ( $M^*$ )/impedance ( $Z^*$ ), tangent-loss ( $\tan\delta$ ), and ac conductivity ( $\sigma_{ac}$ ) of the Al/(S:DLC)/p-Si/Au (MIS)-type Schottky structures in a wide range of frequency and voltage at room temperature (RT)

A. Eroğlu Tezcan <sup>c</sup>, Sabreen A.hameed <sup>a</sup>, A. Feizollahi Vahid <sup>b</sup>, M. Ulusoy <sup>c,\*</sup>, §. Altindal <sup>c</sup>

<sup>a</sup> Department of Physics, College of Science, University of Diyala, Diyala, Iraq

<sup>b</sup> Department of Nanotechnology Engineering, Bülent Ecevit University, 67100, Zonguldak, Turkey

<sup>c</sup> Department of Physics, Faculty of Sciences, Gazi University, 06500, Ankara, Turkey



## ARTICLE INFO

### Keywords:

S-doped DLC Schottky interface  
Dielectric properties  
Electric modulus  
Maxwell-Wagner-type polarization  
AC conductivity

## ABSTRACT

In this work, the Al/(S:DLC)/p-Si/Au Schottky structures were fabricated, and the real and imaginary parts of complex-permittivity ( $\epsilon^*$ ), complex electric-modulus ( $M^*$ ), complex-impedance ( $Z^*$ ), loss-tangent ( $\delta$ ), electrical-conductivity ( $\sigma_{ac}$ ), and phase-angle ( $\theta$ ) were investigated in the wide-frequency-range of **2 kHz-2 MHz** between -3.0V/4.0V. All these-factors were found to be heavily dependent on frequency and voltage because of the surface states ( $N_{ss}$ ), Maxwell-Wagner polarization, and interlayer. The voltage-dependent profile of  $\tan\delta$  and  $M'$  exhibits a significant shift in peak location towards forward-bias voltages as frequency increases due to the relaxation process of the  $N_{ss}$  and dipole polarization. The  $\epsilon'$  was found to be 571.81 (at 2 kHz) and 59.72 (at 1 MHz). The value of  $\epsilon'$ , even at 2 kHz, is about 151.5 times higher than the maximum value of traditional SiO<sub>2</sub> (3.8) insulators, and hence, it can be successfully used instead of insulators to store more electric charges or energy.

## 1. Introduction

If a specially designed metal/semiconductor (MS)-type Schottky structure is not utilized, the use of interlayer materials, such as oxides (SiO<sub>2</sub>, SnO<sub>2</sub>, TiO<sub>2</sub>), ferroelectric materials, like Bi<sub>3</sub>Ti<sub>4</sub>O<sub>12</sub> and STO, as well as pure and doped metal or metal oxide doped materials (Zn, Cu, Ni, MnO, ZnO, CuO), and organic materials (PVA, PVP, etc.) grown by various techniques may lead to the likelihood of  $N_{ss}$  or dislocations occurring during the cleaning and fabrication processes of the semiconductor surface [1–9]. The growth of interlayers between the metal and semiconductor interface through diverse techniques grants them capacitive properties, which facilitate the storage of electronic charges or energy. These interlayers can polarize effortlessly under electric fields in low to intermediate frequencies [10–15]. The performance of these factors depends on various factors, such as the type of interlayer, whether it's native or deposited, its uniformity and thickness, and its dielectric value. Additionally, the form of barrier height (BH) at the junction, the  $R_s$ , and the formation and distribution of  $N_{ss}$  between the

interlayer and the semiconductor also impact their performance. Meanwhile, it is essential to consider the frequency, applied electric field, and doping levels of acceptor or donor atoms in a semiconductor as critical parameters [16–21].

The dielectric constant ( $\epsilon' = C/C_0 = \epsilon' \epsilon_0 A/d_i$ ) and energy storage of the MS structure with an interlayer are critical for enhancing the storage capacity of electronic charges or energy. The interlayer thickness ( $d_i$ ) plays a crucial role in this process. However,  $d_i$  is largely determined by the operating voltage and, therefore, cannot be altered. Here, the amount of capacitance for the empty capacitor is represented by  $C_0$ . Currently, the fundamental challenge is to enhance electronic devices by utilizing interfacial layers with high dielectric properties developed through various methods, with the goal of reducing production costs. In recent years, physicists, material scientists, and chemists have sought to reduce  $R_s$ ,  $N_{ss}$ , and leakage current and increase high/ultracapacitor energy storage and low dielectric loss by growing high-dielectric films between metals and semiconductors [9–20,22].

Due to its superior mechanical and physical properties, diamond-like

\* Corresponding author.

E-mail address: [ulusoymurat@gazi.edu.tr](mailto:ulusoymurat@gazi.edu.tr) (M. Ulusoy).

carbon (DLC) was chosen as an interfacial layer and was grown by electrochemical deposition to fabricate M/Insulator/S (MIS) structures. To enhance the performance of these structures, metal (S) was doped into the pure DLC prior to being grown onto the front of the p-Si wafer. Pure DLC or metal-deposited DLC, compared to insulators, provides several advantages, including high-temperature endurance and high dynamic strength. Carbon is an exceptionally significant and exclusive chemical element, given its ability to transform into up to 32 different types of allotropes. These include graphite and diamond, which correspond to  $sp^2$  and  $sp^3$  orbital hybridization, respectively [9,20,23–28].

In this study, a sulfur-doped DLC film was electrochemically deposited onto a p-Si wafer as an interfacial layer for the purpose of creating an MIS-type structure interlaid with S-DLC. To provide a more detailed, accurate, and reliable analysis of the fundamental dielectric properties, conduction mechanisms, and polarization processes, we conducted dielectric impedance measurements, including ( $\epsilon'$ -V) and ( $\epsilon''$ -V) measurements, in the frequency range of 2 kHz-2 MHz and voltage range of -3V/4V at RT and all these parameters were found to be heavily dependent on frequency and voltage, especially at lower and moderate frequencies in the depletion regime. The real value of dielectric constant ( $\epsilon'$ ) was found as 579.8 for 2 kHz and 30.6 for 2 MHz. This value is almost 152.6 times higher than that of the conventional  $SiO_2$  insulator, even at 2 kHz. Consequently, it is possible for it to store more electronic charges or energy, much like an ultracapacitor. Due to this, the oxide interlayer can potentially replace the use of S-doped DLC films or act as an interfacial layer in the upcoming years.

## 2. Experimental details

In the present work, M/S-doped DLC/S (MIS) type Schottky-structures/diodes (SDs) have been fabricated on the p-Si wafer, which has  $<100>$  float-zone, at about 300  $\mu m$  thickness, 1  $\Omega cm$  resistance, and 2 inches (5.08 cm) diameter. Before the fabrication processes, the wafer was immersed in a 5 % hydrofluoric acid (HF) solution to get rid of the native insulator layer on the semiconductor surface and subsequently cleaned in ethanol and rinsed in deionized water at 5 min ultrasonically. After cleaning processes, Au has high purity (99.999 %) was thermally grown on the whole backside of the wafer at micro-Torr to get good/low-resistivity, an ohmic back contact, and then was annealed at 550 °C in the nitrogen ( $N_2$ ) ambient. After depositing a nanocomposite thin film of S-doped DLC onto a p-Si wafer utilizing the electrochemical method with a precursor mixture of thiophuran and methanol in a ratio of 1:15, the thickness of the film was determined to be 3  $\mu m$  using scanning electron microscopy (SEM). In this study, the electrolytic cell system has already been reported in Elsevier in detail [29]. Finally, high purity Al (99.999 %) was also grown onto (S:DLC) interlayer at  $10^{-6}$  Torr. For additional information regarding the manufacturing processes and the utilization of the electrochemical method, please refer to the references provided [29,30]. In order to get more details on the dielectric features,  $M'$  and  $M''$ , and ac conductivity, the C/G-V data of the sample were analyzed in the frequency range of 2 kHz-2 MHz and voltage range of -3.0V/4.0V by utilizing HP 4192 LF impedance analyzer.

## 3. Result and discussions

### 3.1. SEM analysis of the S doped DLC film

Fig. 1 displays a scanning electron microscope image of the sulfur-doped diamond-like carbon film. The image demonstrates that the p-type silicon wafer was entirely coated with a smooth, continuous, and uniform film without any cracks. This study shows that manipulating the deposition parameters led to the successful production of crack-free films.

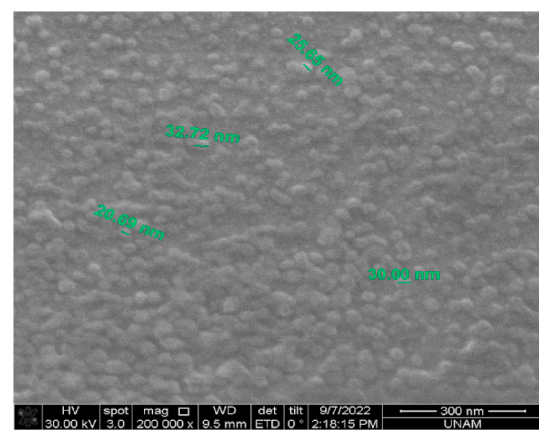


Fig. 1. SEM image of S-DLC nanocomposite film.

### 3.2. XPS analysis

Fig. 2 (a) and (b) display the XPS spectra for C 1s and S 2p of the film. The C 1s spectrum was divided into three different peaks corresponding to C-S, C-C, and C-OOH, respectively [28], as observed in Fig. 2(a). The S 2p spectrum was identified at 167.8 eV and referred to sulfide compounds such as C-S-C and H<sub>2</sub>S [29]. These findings demonstrate that the S was homogeneously doped into the DLC film.

### 3.3. Frequency and voltage dependency of the dielectric characteristics of the structure

The admittance/impedance ( $Y^* = 1/Z^*$ ) spectroscopy method is a crucial and dependable tool to analyze the electrical and dielectric properties of electronic structures with MIS type, with regard to frequency and electric field/voltage [31]. This technique involves a comprehensive range of C/G-V curves at varied frequencies and voltages, and so  $\epsilon'$ ,  $\epsilon''$ ,  $\tan\delta$ ,  $M'$ ,  $M''$  and  $\sigma_{ac}$  values of the MIS type structure can be extracted by using the following relations [4,7,11–13,31]:

$$\epsilon^*(f) = \epsilon'(f) - j\epsilon''(f) = \frac{Cd_i}{\epsilon_o A} - j\frac{Gd_i}{\epsilon_o \cdot 2\pi f \cdot A} = C \left/ \right. C_o - j(G / 2\pi f \cdot C_o) \quad (1a)$$

$$\tan\delta(\omega) = \frac{\epsilon''(\omega)}{\epsilon'(\omega)} \quad (1b)$$

$$M^*(f) = M'(f) + jM''(f) = \frac{\epsilon'(f)}{\epsilon'^2(f) + \epsilon''^2(f)} + j\frac{\epsilon''(f)}{\epsilon'^2(f) + \epsilon''^2(f)} \quad (1c)$$

$$\sigma_{ac}(\omega) = \left( \frac{d_i}{A} \right) \omega C \tan\delta = \epsilon'' \omega \epsilon_0 \quad (1d)$$

in Eq. 1(a-d); the quantities of  $j$ ,  $\omega$ , and  $d_i$  represent the imaginary unit, angular frequency ( $=2\pi f$ ), and interlayer thickness, respectively. Additionally,  $C_0$  denotes the empty capacitor ( $=\epsilon_0 A/d_i$ ). The values of  $\epsilon'$ ,  $\epsilon''$ , and  $\tan\delta$  were determined by measuring the  $C$  and  $G$  values against voltage using Eq. (1a) and (b). These values were plotted in Fig. 3(a-c).

Based on Fig. 3(a), the  $\epsilon'$  vs.  $V$  plots exhibits a clear anomalous peak in the forward-bias region. It is evident that the peak value decreases as the frequency increases. Additionally, the peak position shifts towards the inversion region due to the unique distribution of  $N_{ss}$  at the (S:DLC)/p-Si interface, along with the restructuring and reordering of energy bandgap under voltage effect [1,6–13]. The  $\epsilon''$  vs.  $V$  plots in the same voltage range in Fig. 3(b) shows an increase as voltage increases, and the maximum value of  $\epsilon''$  corresponds to the minimum value of  $\epsilon'$ . This behavior is known as inductive behavior and occurs when samples behave like a conductive material after a certain forward-bias voltage. In other words, the negative differential conductance of  $\epsilon'$  is evident in the

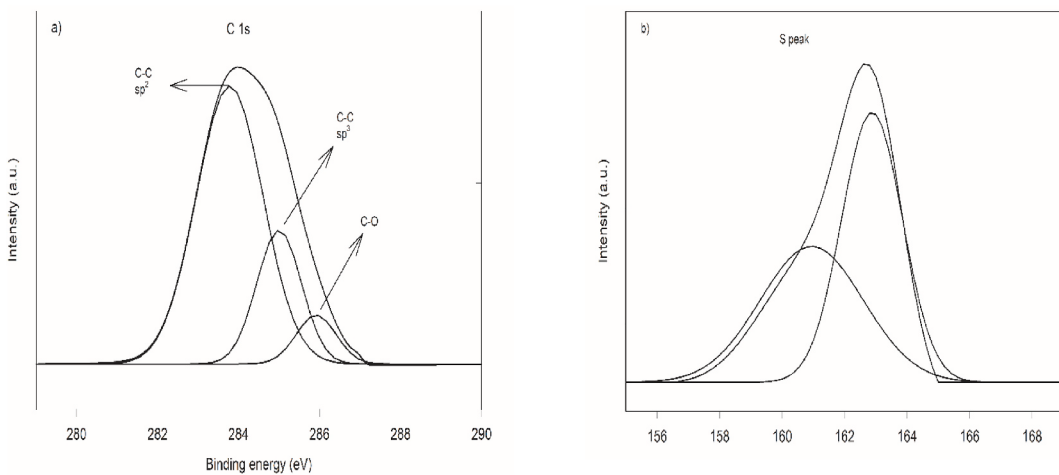


**Fig. 2.** (a) and (b) show the C 1s and S 2p XPS spectra of the film.

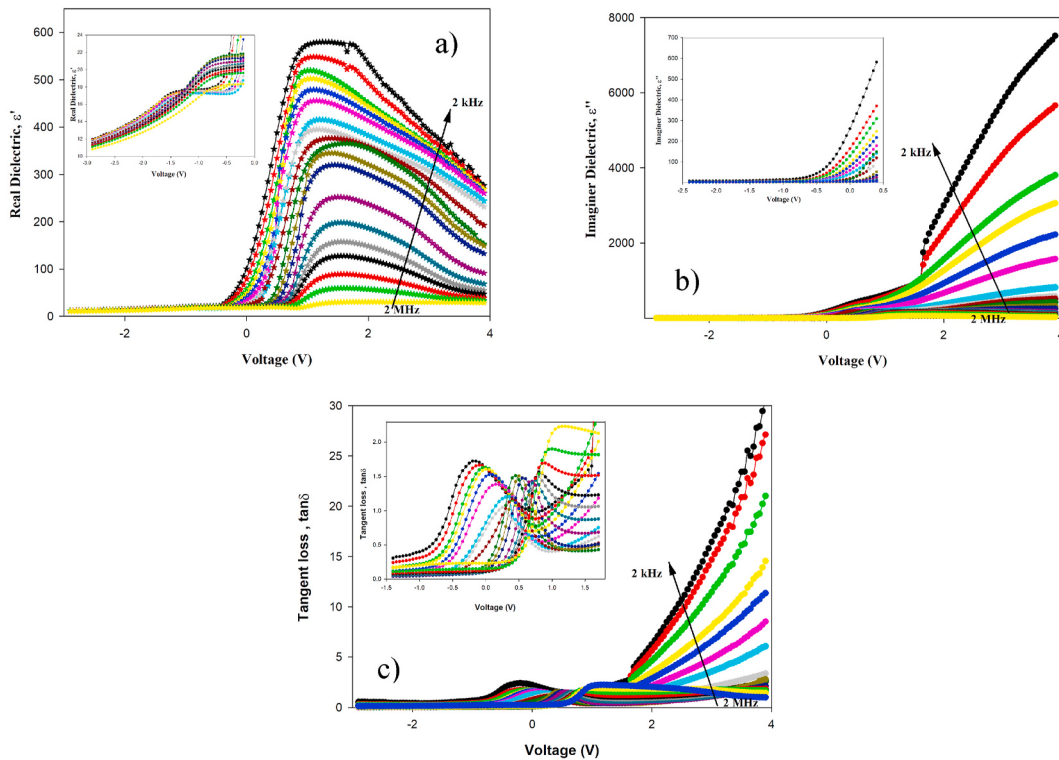


**Fig. 3.** a)  $\epsilon'$ -V, b)  $\epsilon''$ -V, and c)  $\tan\delta$ -V plots of the M/S-doped DLC/S structure.

positive voltage range due to the presence of  $R_s$ , inter-layer, and decreased electronic charges between the two electrodes.

As depicted in Fig. 3(c), the  $\tan\delta$  vs. V plots show a peak for every frequency, and these peaks shift towards the accumulation region based on a particular distribution of  $N_{ss}$  that depends on their lifetimes and the dielectric relaxation that occurs in the interlayer, commonly referred to as the Maxwell-Wagner polarization phenomenon [5,18,22,32]. Electric fields induce polarization in interlayers, including surface or interfacial, dipole, electronic, and ionic or atomic-type polarizations. The first two types can occur only at low and moderate frequencies, while the last two types occur only at high frequencies ( $10^{10}$ – $10^{15}$  Hz). These parameters were plotted in a voltage range (0–3 V), which encompasses both depletion and accumulation regions as a function of frequency. (see Fig. 4(a–c)).

As it appears from Fig. 4(a–c), the values of  $\epsilon'$  and  $\epsilon''$  decrease with

increase almost as exponentially for each applied bias voltage. On the other hand, the values of  $\tan\delta$  give rise to a broad peak (Fig. 4(c)) and exhibit a crossing behavior at higher frequencies, which is attributed to the polarization effects and surface states decreasing and not contributing any excess value to the measurement of the  $\epsilon'$  and  $\epsilon''$ . Dielectric materials, including insulators, ferroelectrics, and pure or dopant polymers/organics, are known to easily polarize under an external electric field. This polarizing effect causes the position of carriers to change from one trap to another and rotate around themselves when given enough time. In other words, the fluctuation of dielectric parameters with the applied electric field and frequency due to relaxation time, particularly at low and moderate frequencies, leads to an excess dielectric constant relative to the actual parameter value [5]. Higher storage of electronic charges or energy in MIS-type capacitors can be achieved through the use of a high dielectric interfacial layer and by

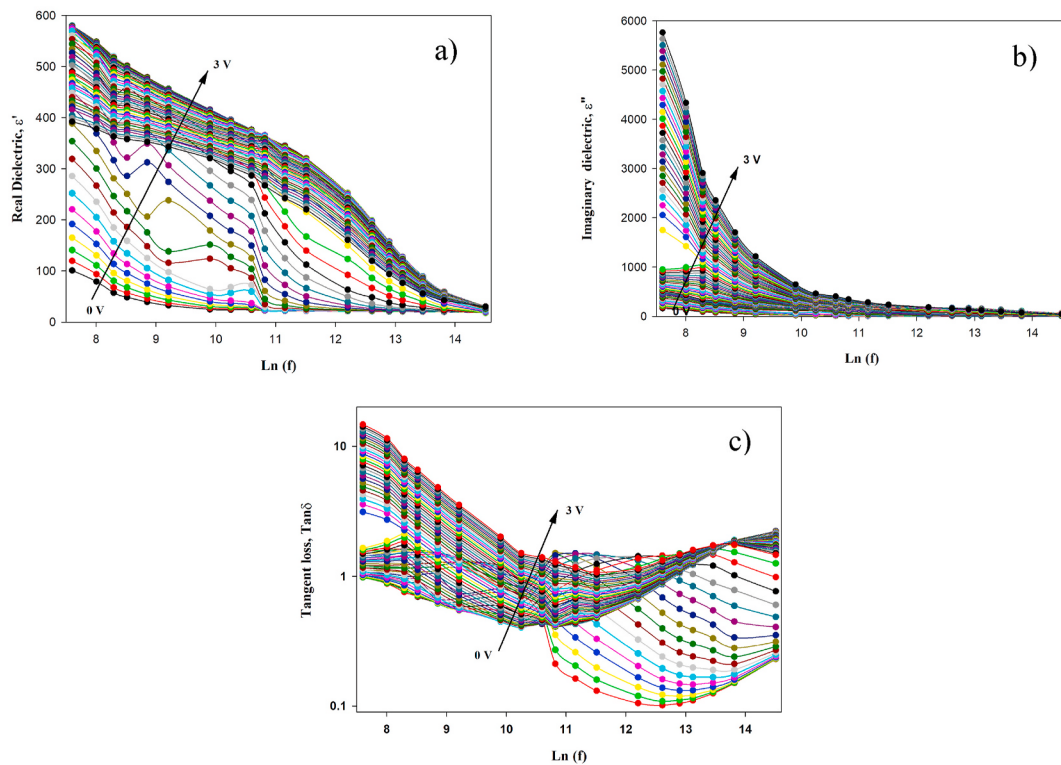


**Fig. 4.** a)  $\epsilon'$ - $\text{Ln}(f)$ , b)  $\epsilon''$ - $\text{Ln}(f)$ , and c)  $\tan\delta$ - $\text{Ln}(f)$  plots of the M/S-doped DLC/S structure.

decreasing its thickness ( $d_i$ ). However, reducing the thickness of the interlayer and increasing the rectifier contact area ( $A$ ) do not yield any advantage in nanostructures. Therefore, we can successfully explain the changes in dielectric properties with electric field and frequency in this study (2 kHz - 2 MHz) based on the relaxation time. Before the direction of the electric field changes, dipoles align with it, causing an increase in the values of  $\epsilon'$  and  $\epsilon''$  [5,8,9,13].

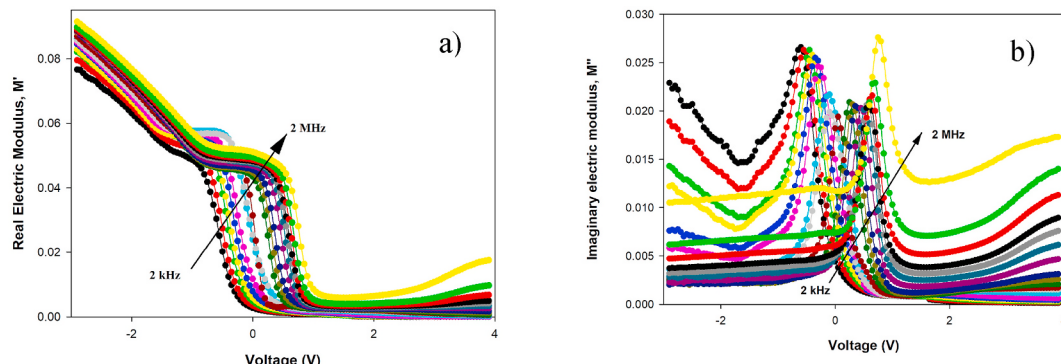
From Eq. (1c),  $M'$  and  $M''$  values were extracted, denoted in Fig. 5(a) and (b) using  $\epsilon'$  and  $\epsilon''$ .

Fig. 5(a) demonstrates that the  $M'$  values generally decrease with increasing voltage; however, the plots of  $M''$  vs.  $V$  exhibit peaks for each frequency (see Fig. 5(b)). Specifically, the position of the peak shifted from  $-0.60$  V (at 2 kHz) to  $0.75$  V (at 2 MHz), and the magnitude of the peak varies across different regions due to surface states, relaxation times, and Maxwell-Wagner polarization [20,22,33,25]. The movement of electronic charges over long distances is another factor contributing to the observed peak in the  $M''$  vs.  $V$  plots for each frequency.

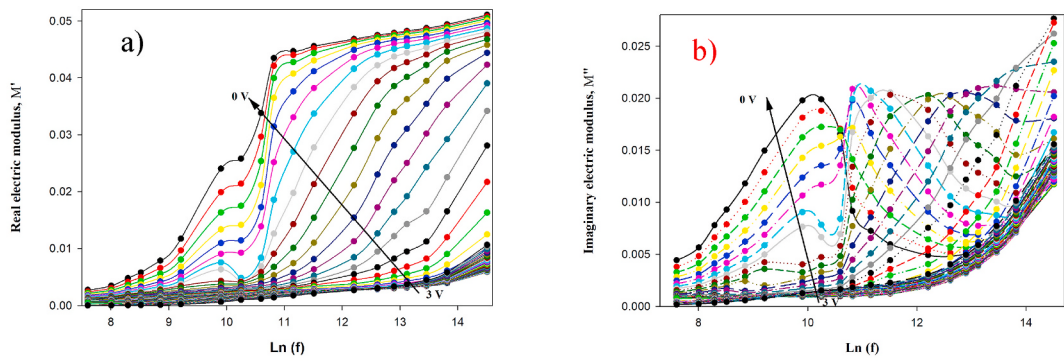
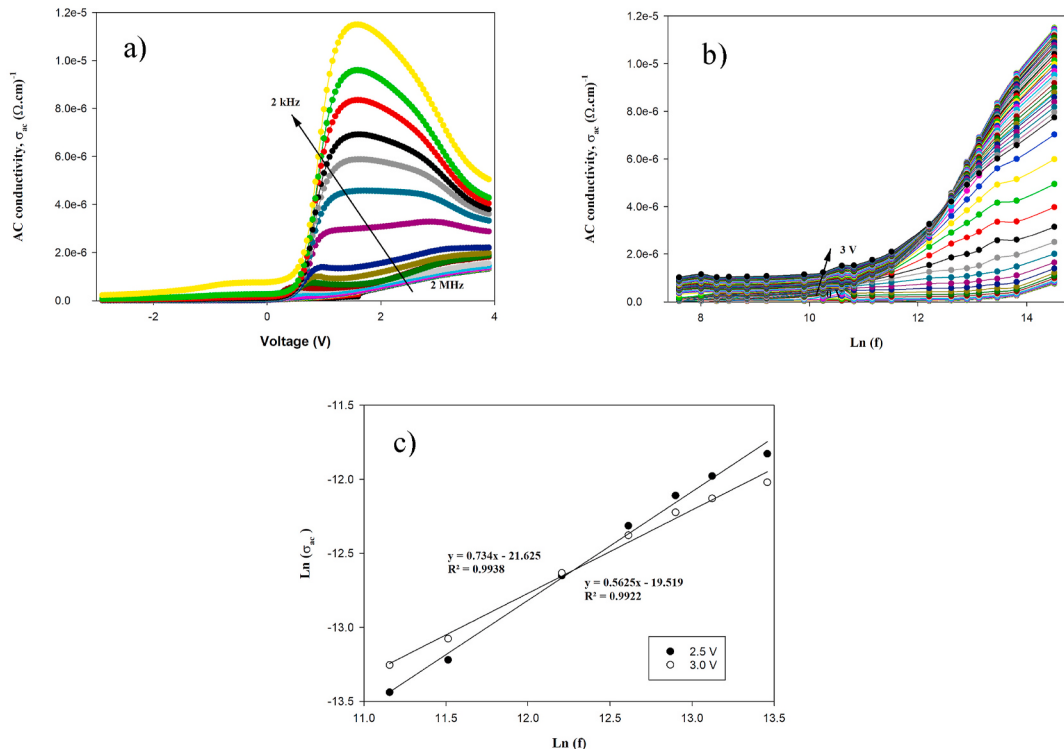
It is shown in Fig. 6 (a) and (b) to observe the frequency-dependent changes of  $M'$  and  $M''$  in response to voltage variations between 0 and 3V

at 50 mV steps. As shown in Fig. 6(a), the actual electric modulus ( $M'$ ) value varies depending on frequency and decreases with voltage in the depletion-accumulation zones due to a change in conduction phenomena resulting from electrons' limited mobility range. At low frequencies, both  $M'$  and  $M''$  values approach zero due to a decrease in surface and dipole polarization as well as the effects of interface traps. In other words, the highest possible value of  $M'$  corresponds to  $M_\infty = 1/\epsilon_\infty$  due to relaxation processes and so the relaxation time ( $\tau$ ) possible to find from the peak value of  $M'$  using  $\omega_{\max}\tau = 1$  relation [23]. Thus, the value of  $\tau$  was found as  $7.99$   $\mu$ s at zero bias voltage.

The function of voltage and frequency, the value of ac electrical-conductivity ( $\sigma_{ac} = \epsilon''\omega\epsilon_0$ ) for the M/S-doped DLC/S structure was determined as illustrated in Fig. 7(a) and (b). Fig. 7(a) illustrates that  $\sigma_{ac}$  values increase with rising voltage until the accumulation region and then decrease with further voltage increase, particularly at low and moderate bias voltage. On the other hand, Fig. 7(b) shows that the semilogarithmic plot ( $\sigma_{ac}$  vs.  $\text{Ln}(f)$ ) for forward bias voltages is almost frequency-independent, with a plateau evident at both moderate and low frequencies. However, at higher frequencies, this plot increases



**Fig. 5.** a)  $M'$ - $V$  and b)  $M''$ - $V$  plots of the M/S-doped DLC/S structure.

Fig. 6. a)  $M'$ -ln( $f$ ) and b)  $M''$ -ln( $f$ ) plots of the M/S-doped DLC/S structure.Fig. 7. a)  $\sigma_{ac}$ -V, b)  $\sigma_{ac}$ - $\ln(f)$ , and c)  $\ln(\sigma_{ac})$ - $\ln(f)$  plots of the M/S-doped DLC/S structure.

almost exponentially. This low-moderate frequency range corresponds to dc-conductivity ( $\sigma_{dc}$ ), whereas at higher frequencies range is equivalent to ac conductivity.

Fig. 7(c) demonstrates that the double-logarithmic  $\sigma_{ac}$ - $f$  plot follows a power-law dependence on frequency [34]:

$$\sigma(\omega) = \sigma_{dc} + A\omega^n \quad (2)$$

where  $A$  is a constant and  $n$  is the slope of the double logarithmic  $\sigma_{ac}$ - $f$  plot for the specified applied bias voltage. Thus, according to Fig. 7(c), the slope of the  $\ln(\sigma_{ac})$  vs.  $\ln(f)$  plots for 2.5 V and 3.0 V have good liner behavior with 0.734 and 0.563, respectively. When  $n$  is less than 1, the hopping mechanism involves sudden hopping accompanied by translational motion. Moreover, these results indicate significant differences in the conduction mechanism of the structure between the low to moderate and high frequency ranges.

The dielectric behavior and relaxation of the MIS-type structure can be determined through impedance spectroscopy using the relations provided by the ISM [12,35]:

$$Z^*(\omega) = Z'(\omega) - jZ''(\omega) = \frac{1}{j\omega C_0 \epsilon^*(\omega)} = \frac{\epsilon''}{\omega C_0 [\epsilon'^2 + \epsilon''^2]} - j \frac{\epsilon'}{\omega C_0 [\epsilon'^2 + \epsilon''^2]} \quad (3)$$

in Eq. (3),  $Z'$  and  $Z''$  stand for the real and imaginary parts of the complex impedance ( $Z^*$ ), respectively. For further insights into the dielectric behavior, refer to Fig. 8(a-d), which showcase  $Z'$  and  $Z''$  vs. voltage and frequency. Although  $Z'$  and  $Z''$  values decrease with increasing frequency, the  $Z'$  vs.  $V$  plots display a clear peak in the reverse bias region, as shown in Fig. 8(a). This occurrence is attributed to the presence of  $N_{ss}$  and fixed electronic charges, and the peak amplitude decreases as the frequency increases. Additionally, the peak's position shifts towards a lower negative voltage point.

The variation of the phase angle ( $\theta$ ) with bias voltage was obtained by utilizing the  $Z'$  and  $Z''$  relationship, as illustrated in Fig. 9 for each frequency.

$$\theta = \tan^{-1} \left( \frac{Z''}{Z'} \right) \quad (4)$$

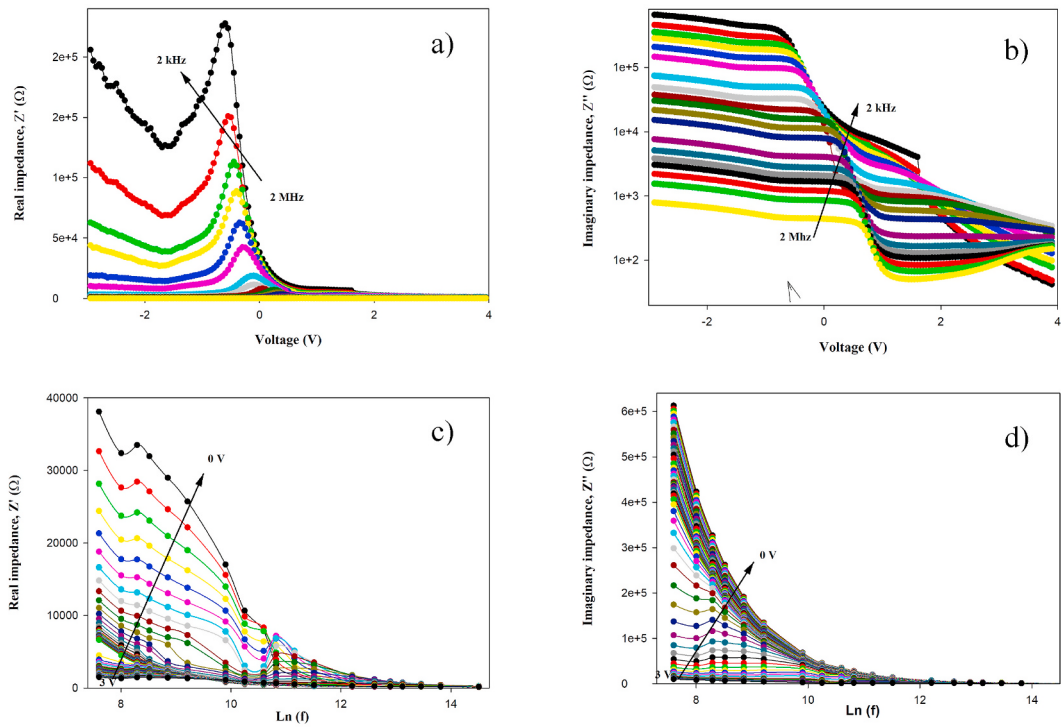


**Fig. 8.** a)  $Z'$ - $V$ , b)  $Z''$ - $V$ , c)  $Z'$ - $\ln(f)$ , and d)  $Z''$ - $\ln(f)$  plots of the M/S-doped DLC/S structure.

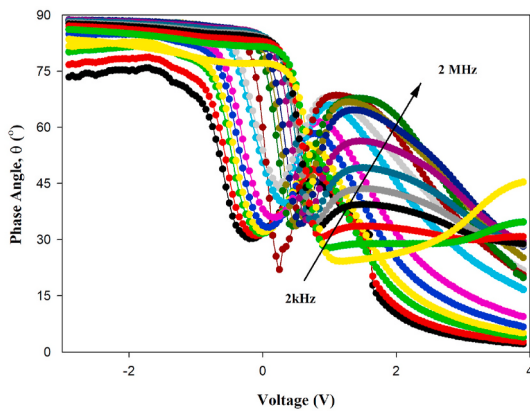


**Fig. 9.** The changes in the phase-angle in the frequency range of 2 kHz- 2 MHz.

As depicted in the figure, the interfacial layer (S-doped DLC) displays a purely capacitive behavior, as evidenced by the phase angle value remaining constant at around  $90^{\circ}$  in the negative voltage region [12,35]. The capacitive behavior in the interfacial layer can be defined by the phase angle, which approaches zero at low frequencies.

The experimental results reveal that numerous factors, such as interlayers between the interface, their thickness, polarization processes, hopping mechanisms, interface states/traps, their lifetimes ( $\tau$ ), frequency, and voltage, affect the dielectric characteristics,  $M'$ ,  $M''$ , and ac conductivity of MS-type structures with or without an interlayer. The presence of charges at traps contributes considerably to the polarization processes, particularly at low and midrange frequencies within the depletion region. However, this effect can be disregarded at higher frequencies ( $f \geq 1$  MHz) [27]. Since trapped electrons and dipoles can be reorganized and rearranged under the influence of an electric field, interface, and dipole polarization can occur at low frequencies up to a few kHz. Because at higher frequencies, the dipoles have less time to align, resulting in a decrease in the dielectric constant [5].  $Z$ - $V$ - $f$

measurements were conducted in the frequency range of 2 kHz - 2 MHz in this study. This frequency range may have a greater effect on interfacial and dipole polarizations. Similar results on the frequency and voltage-dependent electric and dielectric properties have been previously reported in the literature by various researchers over the last decade [32,34-38].

**Fig. 10(a-d)** illustrates the  $Z''$  vs.  $Z'$  curves for the structure at room temperature across frequencies of 1 kHz, 10 kHz, 100 kHz, and 1 MHz in the  $-3/4$  V range. It is evident from this representation that the  $Z''$  vs.  $Z'$  curves exhibit a distinct semicircular or peak shape across all frequencies, with the peak value decreasing swiftly as the frequency increases. The observed semicircle for four different frequencies and their radius were chosen based on the  $Z'$  axis. The observed behavior elucidates the rapid diminishing of polarization or relaxation processes with increasing frequency. In essence, the curves demonstrate that frequency has a substantial impact on the dielectric properties.

When cole-cole plots are obtained from the impedance measurements for any constant voltage, the situation may be considerably different. In addition, **Fig. 11(a-b)** shows  $Z'$  vs  $Z''$  plots for two different voltages (-3 and +3 V). These plots demonstrate that Cole-Cole plots have a nearly semicircular shape. It is obvious that the total impedance and the radius of the semicircles vary significantly depending on the voltage. As expected, the impedance values and radius are high in the reverse bias. These changes can be described by the equivalent circuit of the resistance and capacitance combinations of the structure. In **Fig. 11(b)**, the equivalent circuit is shown. The substrate resistance represents the series resistance ( $R_s$ ), while the surface states located between the semiconductor and the interfacial layer represent the first network ( $R_1//C_1$ ). The interfacial layer represents the second network ( $R_2//C_2$ ) [39].

#### 4. Conclusion

This study focuses on the frequency/voltage dependence of the prepared M/S-doped DLC/S (MIS type) structure's  $\epsilon^*$ ,  $M^*$ ,  $\tan\delta$ , and  $\sigma_{ac}$  values using the impedance spectroscopy method. The measurements were executed within the frequency range of 2 kHz - 2 MHz and the voltage range of -3V/+4V. Due to Maxwell-Wagner relaxation

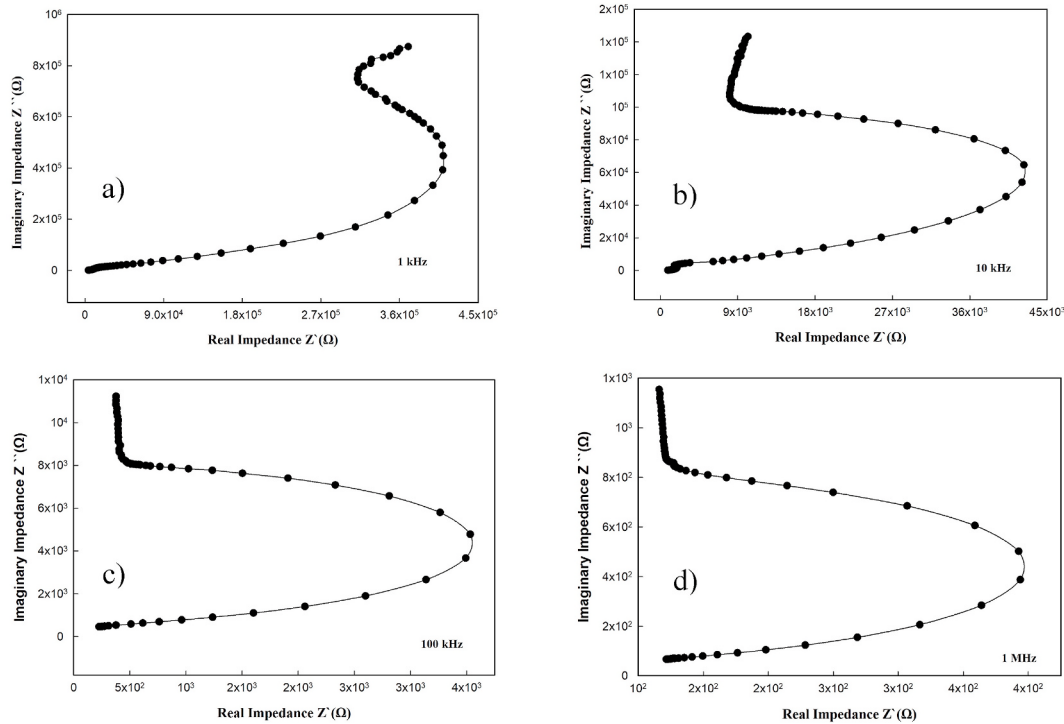


**Fig. 10.** (a–d) The  $Z''$  vs  $Z'$  plots of the M/S-doped DLC/S structure at certain frequencies.

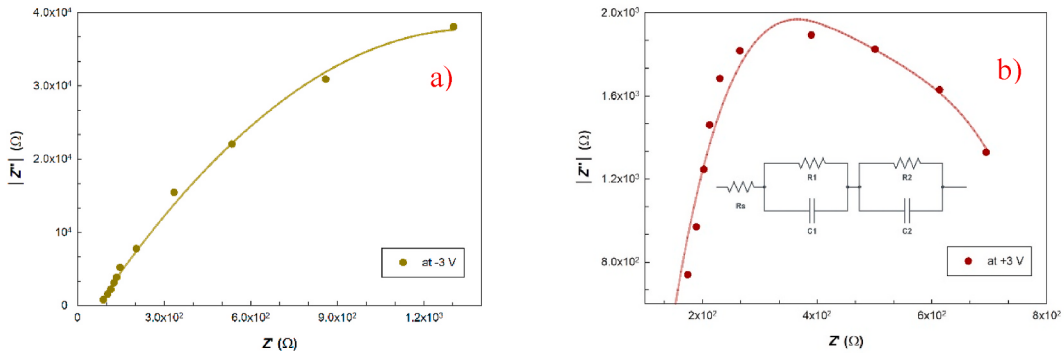


**Fig. 11.** (a–b) The  $Z''$  vs  $Z'$  plots of the M/S-doped DLC/S structure at certain voltages.

processes, the parameters of  $N_{ss}$  and  $R_s$  were found to be heavily reliant on the variables of  $f$  and  $V$  in the depletion and accumulation regions. The increased values of  $\epsilon'$  and  $\epsilon''$  at lower frequencies are a result of the special distribution of  $N_{ss}$  at the interface of (S-DLC)/p-Si. The polarization of the interface and dipole relies on the relaxation time for lower frequencies, as opposed to the period ( $T = 1/2\pi f$ ). The higher values of  $M'$  and  $M''$  were obtained due to the considerable mobility of carriers over long distances, as evidenced by the distinct peak on the  $M''$  vs  $V$  plots for each frequency. The peak position shifted from  $-0.60$  V at  $2$  kHz to  $0.75$  V at  $2$  MHz, attributable to the extended mobility possibilities of electronic charge carriers. The value of phase angle ( $\theta$ ) remains almost constant at about  $90^\circ$  for the negative voltage region and than which indicated that the interfacial (S-doped DLC) layer exhibits a pure capacitive behavior. Maxwell-Wagner polarization is believed to be a dispersion that occurs in the complex dielectric and complex electric modulus, particularly at low and intermediate frequencies. The characteristics of  $Z''$  vs  $Z'$  demonstrate a rapid decrease in polarization or relaxation processes as frequency increases. The  $Z''$  vs  $Z'$  curves show that frequency has a significant influence on dielectric properties. Overall, the  $\epsilon'$  values were found to be  $571.81$  (at  $2$  kHz) and  $59.72$  (at  $1$  MHz),

respectively. This indicates that the  $\epsilon'$  value is  $151.5$  times greater than the maximum value for  $\text{SiO}_2$  ( $3.8$ ), even at  $2$  kHz. Therefore, it has the potential to replace insulators for more efficient electrical charge and energy storage.

#### CRediT authorship contribution statement

**A. Eroglu Tezcan:** Writing – original draft, Data curation. **Sabreen A.hameed:** Software, Data curation. **A. Feizollahi Vahid:** Resources, Methodology. **M. Ulusoy:** Writing – original draft, Data curation. **Ş. Altindal:** Writing – review & editing, Supervision.

#### Declaration of competing interest

The authors declare that they have no known competing financial interests or personal relationships that could have appeared to influence the work reported in this paper.

## Data availability

Data will be made available on request.

## References

- [1] V. Rajagopal Reddy, C. Venkata Prasad, Surface chemical states, electrical and carrier transport properties of Au/ZrO<sub>2</sub>/n-GaN MIS junction with a high-k ZrO<sub>2</sub> as an insulating layer, *Mater. Sci. Eng. B* 231 (2018) 74–80.
- [2] M. Sharma, S.K. Tripathi, Frequency and voltage dependence of admittance characteristics of Al/Al<sub>2</sub>O<sub>3</sub>/PVA:n-ZnSe Schottky barrier diodes, *Mater. Sci. Semicond. Process.* 41 (2016) 155–161.
- [3] H.C. Card, E.H. Rhoderick, Studies of tunnel MOS diodes I. Interface effects in silicon Schottky diodes, *J. Phys. D Appl. Phys.* 4 (1971) 1589.
- [4] C.V. Subba Reddy, X. Han, Q.-Y. Zhu, L.-Q. Mai, W. Chen, Dielectric spectroscopy studies on (PVP+PVA) polyblend film, *Microelectron. Eng.* 83 (2006) 281–285.
- [5] H.N. Chandrakala, B. RamarajShivakumaraiah, G.M. Madhu, Siddaramaiah, the influence of zinc oxide–cerium oxide nanoparticles on the structural characteristics and electrical properties of polyvinyl alcohol films, *J. Mater. Sci. Mater. Electron.* 47 (2012) 8076–8084.
- [6] B.J. Madhu, *Emergent Research on Polymeric and CompositeMaterials*, IGI Global, Hershey, 2018, pp. 209–224.
- [7] Q. Liu, X. Zhu, Z. Huo, X. He, Y. Liang, M. Xu, Electrochemical detection of dopamine in the presence of ascorbic acid using PVP/graphene modified electrodes, *Talanta* 97 (2012) 557–562.
- [8] O. Sevgili, On the examination of temperature-dependent possible current-conduction mechanisms of Au/(nanocarbon-PVP)/n-Si Schottky barrier diodes in wide range of voltage, *J. Mater. Sci. Mater. Electron.* 32 (2021) 10112–10122.
- [9] A. Feizollahi Vahid, S. Alptekin, N. Basman, M. Ulusoy, Y. Şafak Asar, Ş. Altindal, The investigation of frequency dependent dielectric properties and ac conductivity by impedance spectroscopy in the Al/(Cu-doped Diamond like Carbon)/Au structures, *J. Mater. Sci. Mater. Electron.* 34 (2023) 1118.
- [10] N. Kumar, S. Chand, Effects of temperature, bias and frequency on the dielectric properties and electrical conductivity of Ni/SiO<sub>2</sub>/p-Si/Al MIS Schottky diodes, *J. Alloys Compd.* 817 (2020) 153294.
- [11] S. Basha, G.S. Sundari, K.V. Kumar, M.C. Rao, Structural and dielectric properties of PVP based Composite polymer electrolyte thin films, *J. Inorg. Organomet. Polym. Mater.* 27 (2017) 455–466.
- [12] A.M. Akbaş, A. Tataroğlu, Ş. Altindal, Y. Azizian-Kalandaragh, Frequency dependence of the dielectric properties of Au/(NG:PVP)/n-Si structures, *J. Mater. Sci. Mater. Electron.* 32 (2021) 7657–7670.
- [13] C.P. Smyth, *Dielectric Behaviour and Structure*, McGraw-Hill, New York, 1995.
- [14] Y. Slimani B. Unal, E. Hannachi, A. Selmi, M.A. Almessiere M. Nawaz, A. Baykal, M. Yıldız, Frequency and dc bias voltage dependent dielectric properties and electrical conductivity of BaTiO<sub>3</sub> single bondSrTiO<sub>3</sub>/(SiO<sub>2</sub>)<sub>x</sub> nanocomposites, *Ceram. Int.* 45 (2019) 11989–12000.
- [15] A. Barkhordari, H. Mashayekhi, P. Amiri, Ş. Altindal, Y. Azizian-Kalandaragh, On the investigation of frequency-dependent dielectric features in Schottky barrier diodes (SBs) with polymer interfacial layer doped by graphene and ZnTiO<sub>3</sub> nanostructures, *Appl. Phys. A* 129 (2023) 249.
- [16] H.G. Çetinkaya, Frequency and voltage dependent profile of dielectric parameters and electric modulus for Al/(HgS-PVA)/p-Si Capacitor via impedance Spectroscopy method, *J. Nanoelectron. Optoelectron.* 13 (2018) 421–427.
- [17] V. Manjunath, V.R. Reddy, P.R.S. Reddy, CJ Choi Vjamardhanam, Electrical and frequency-dependent properties of Au/Sm<sub>2</sub>O<sub>3</sub>/n-GaN MIS junction with a high-k rare-earth Sm<sub>2</sub>O<sub>3</sub> as interlayer, *Curr. Appl. Phys.* 17 (2017) 980–988.
- [18] S. Demirezen, A. Eroğlu, Y. Azizian-Kalandaragh, Ş. Altindal, Electric and dielectric parameters in Au/n-Si (MS) capacitors with metal oxide-polymer interlayer as function of frequency and voltage, *J. Mater. Sci. Mater. Electron.* 31 (2020) 15589–15598.
- [19] A. Dutta, C. Bharti, T.P. Sinha, AC conductivity and dielectric relaxation in CaMg1/3Nb2/3O<sub>3</sub>, *Mater. Res. Bull.* 43 (2008) 1246–1254.
- [20] Ö. Berkün, M. Ulusoy, Ş. Altindal, B. Avar, On frequency and voltage dependent physical characteristics and interface states characterization of the metal semiconductor (MS) structures with (Ti: DLC) interlayer, *Phys. B Condens. Matter* 666 (2023) 415099.
- [21] M.S. Pratap Reddy, L. Jung-Hee, J. Ja-Soon, Frequency dependent series resistance and interface states in Au/bio-organic/n-GaN Schottky structures based on DNA biopolymer, *Synth. Met.* 185 (2013) 167–171.
- [22] T. Tunç, H. Uslu, Ş. Altindal, Preparation and dielectric properties of polyvinyl alcohol (Co, Zn Acetate) Fiber/n-Si and polyvinyl alcohol (Ni, Zn Acetate)/n-Si Schottky diodes, *Fibers Polym.* 12 (2011) 886.
- [23] A. Zkria, E. Abubakr, P. Sittimart, T. Yoshitake, Analysis of electrical characteristics of Pd/n-Nanocarbon/p-Si heterojunction diodes: by C-V-f and G/w-V-f, *J. Nanomater.* 9 (2020) 4917946, <https://doi.org/10.1155/2020/4917946>.
- [24] S. Koizumi, H. Umezawa, J. Pernot, M. Suzuki, *Power Electronics Device Applications of Diamond Semiconductors*, Woodhead Publishing, United Kingdom, 2018.
- [25] M. Shaban, A. Zkria, T. Yoshitake, Temperature-Dependent Impedance Spectra of Nitrogen-Doped Ultrananocrystalline Diamond Films Grown on Si Substrates, vol. 9, 2021, pp. 896–904.
- [26] S. Wan, L. Wang, Q. Xue, Electrochemical deposition of sulfur doped DLC nanocomposite film at atmospheric pressure, *Electrochim. Commun.* 12 (2010) 61–65.
- [27] W. Xu, K. Zhou, S. Lin, M. Dai, Q. Shi, C. Wei, Structural properties of hydrogenated Al-doped diamond-like carbon films fabricated by a hybrid plasma system, *Diamond Relat. Mater.* 87 (2018) 177–185.
- [28] M.S. Kurt, F. Yıldırım, Z. Orhan, S. Aydoğan, Influence of thickness of the sputtered diamond-like carbon (DLC) on electronic and dielectric parameters of the Au/DLC/n-Si heterojunction, *J. Mater. Sci. Mater. Electron.* 32 (2021) 25214–25224.
- [29] X. Yan, T. Xu, G. Chen, S. Yang, H. Liu, Study of structure, tribological properties and growth mechanism of DLC and nitrogen-doped DLC films deposited by electrochemical technique, *Appl. Surf. Sci.* 236 (2004) 328–335.
- [30] N. Basman, S. Fiat Varol, High temperature characterization of a MIS Schottky diode based on diamond-like carbon nanocomposite film, *J. Electron. Mater.* 48 (2019) 7874–7881.
- [31] A. Chelkowski, *Dielectrics Physics*, PWN/Elsevier, Amsterdam, 1980.
- [32] G.A. Kontos, A.L. Soulintzis, P.K. Karahaliou, G.C. Psarras, S.N. Georgia, C. A. Krontiras, M.N. Pisianas, Electrical relaxation dynamics in TiO<sub>2</sub>-polymer matrix composites, *Express Polym. Lett.* 1 (2007) 781–789.
- [33] S. Hilal, A. Farji, N. Hizem, L. Militaru, A. Kalboussi, A. Souifi, High temperature and voltage dependent electrical and dielectric properties of TiN/Al2O3/p-Si MIS structure, *J. Alloys Compd.* 713 (2017) 194–203.
- [34] G. Yelliah, T. Shekharam, K. Hadasa, M. Nagabushanam, Low temperature DC conductivity, impedance spectroscopy and dielectric properties of Na doped Cd<sub>0.8</sub>Zn<sub>0.2</sub>S semiconductor compounds, *J. Alloys Compd.* 609 (2014) 192–200.
- [35] S. Nasri, A. Oueslati, I. Chaabane, M. Gargouri, AC Conductivity, Electric Modulus Analysis and Electrical Conduction Mechanism of RbFeP<sub>2</sub>O<sub>7</sub> Ceramic Compound, vol. 42, 2016, pp. 14041–14048.
- [36] Kaleem Ahmad, Wei Pan, Sui-Lin Shi, Electrical conductivity and dielectric properties of multiwalled carbon nanotube and alumina composites, *Appl. Phys. Lett.* 89 (2006) 133122.
- [37] W. Filali, N. Sengouga, S. Oussalah, R.H. Mari, D. Jameel, N.A. Al Saqri, M. Aziz, D. Taylor, M. Henini, Characterisation of temperature dependent parameters of multi-quantum well (MQW) Ti/Al/n-AlGaAs/n-GaAs/n-AlGaAs Schottky diodes, *Superlattice. Microst.* 111 (2017) 1010–1021.
- [38] S. Altindal Yerişkin, E.E. Tanrikulu, M. Ulusoy, Dielectric properties of MS diodes with Ag: ZnO doped PVP interfacial layer depending on voltage and frequency, *Mater. Chem. Phys.* 303 (2023) 127788.
- [39] Chanyoung Yim, Niall McEvoy, S. Georg, Characterization of graphene-silicon Schottky barrier diodes using impedance spectroscopy, *Appl. Phys. Lett.* 103 (2013) 193106.